Article

Preferential Oxidation of Carbon Monoxide Catalyzed by Platinum Nanoparticles in Mesoporous Silica

Atsushi Fukuoka, Jun-ichi Kimura, Tadashi Oshio, Yuzuru Sakamoto, and Masaru Ichikawa

J. Am. Chem. Soc., **2007**, 129 (33), 10120-10125• DOI: 10.1021/ja0703123 • Publication Date (Web): 31 July 2007

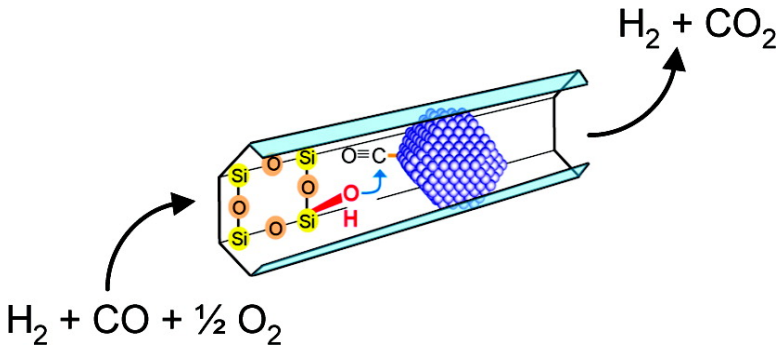

More About This Article

Additional resources and features associated with this article are available within the HTML version:

- Supporting Information
- Links to the 12 articles that cite this article, as of the time of this article download
- Access to high resolution figures
- Links to articles and content related to this article
- Copyright permission to reproduce figures and/or text from this article

View the Full Text HTML

J|A|C|S
ARTICLES
Published on Web 07/31/2007

Preferential Oxidation of Carbon Monoxide Catalyzed by Platinum Nanoparticles in Mesoporous Silica

Atsushi Fukuoka,*,† Jun-ichi Kimura,‡ Tadashi Oshio,‡ Yuzuru Sakamoto,‡ and Masaru Ichikawa†

Contribution from Catalysis Research Center, Hokkaido University, N-21 W-10, Sapporo 001-0021, Japan, and Division of Chemistry, Graduate School of Science, Hokkaido University, N-10 W-8, Sapporo 060-0810, Japan

Received January 15, 2007; E-mail: fukuoka@cat.hokudai.ac.jp

Abstract: Preferential oxidation (PROX) of CO is an important practical process to purify H_2 for use in polymer electrolyte fuel cells. Although many supported noble metal catalysts have been reported so far, their catalytic performances remain insufficient for operation at low temperature. We found that Pt nanoparticles in mesoporous silica give unprecedented activity, selectivity, and durability in the PROX reaction below 353 K. We also studied the promotional effect of mesoporous silica in the Pt-catalyzed PROX reaction by infrared spectroscopy using the isotopic tracer technique. Gas-phase O_2 is not directly used for CO oxidation, but the oxygen of mesoporous silica is incorporated into CO_2. These results suggest that CO oxidation is promoted by the attack of the surface OH groups to CO on Pt without forming water.

1. Introduction

Since the discovery of FSM-16[1,2] and MCM-41[3] in the early 1990s, mesoporous silicas[1−5] have been extensively explored for practical applications in catalysis,[6,7] sorption,[8,9] electronics, and so on.[10] The mesoporous silicas are characterized by ordered pores (2−10 nm) with high surface area (ca. 500−1000 $m^2\ g^{-1}$), which are attractive as catalysts and supports. In the reported works on catalysis, however, the characteristic of high surface area was simply used to give higher dispersion of active sites than that over the conventional silica. The unique promotional effect of the mesoporous silica was described in the literature,[6,7,11−14] but the effect remains unclear at the molecular level.

To design heterogeneous catalysts capable of high activity and selectivity, we have studied the template synthesis of metal nanoclusters in mesoporous silicas.[15−18] In this work, we targeted the preferential oxidation of CO (PROX: $CO + {}^1/_2O_2 \rightarrow CO_2$) in excess H_2 as a catalytic reaction, because the PROX is important for the purification of H_2 for polymer electrolyte fuel cells (PEFCs). H_2 produced from gasoline or natural gas contains a small amount of CO,[19] but CO is a strong poison to Pt electrodes in the PEFCs. Currently, CO is decreased to ca. 10 ppm by the PROX reaction at 423 K, and then H_2 is supplied to the PEFCs at 353 K. If the PROX is operated below 353 K, the number of cooling processes can be reduced in the practical production of H_2. Supported noble metals such as Pt,[20−24] Ru,[25] Au,[26,27] and bimetallic Pt−Fe[28,29] have been reported as the

† Catalysis Research Center.
‡ Division of Chemistry.

(1) Yanagisawa, T.; Shimizu, T.; Kuroda, K.; Kato, C. *Bull. Chem. Soc. Jpn.* **1990**, *63*, 988−992.
(2) Inagaki, S.; Fukushima, Y.; Kuroda, K. *J. Chem. Soc., Chem. Commun.* **1993**, 680−682.
(3) Kresge, C. T.; Leonowicz, M. E.; Roth, W. J.; Vartuli, J. C.; Beck, J. S. *Nature* **1992**, *359*, 710−712.
(4) Zhao, D.; Feng, J.; Huo, Q.; Melosh, N.; Fredrickson, G. H.; Chmelka, B. F.; Stucky, G. D. *Science* **1998**, *279*, 548−552.
(5) Inagaki, S.; Guan, S.; Fukushima, Y.; Ohsuna, T.; Terasaki, O. *J. Am. Chem. Soc.* **1999**, *121*, 9611−9614.
(6) Corma, A. *Chem. Rev.* **1997**, *97*, 2372−2419.
(7) Thomas, J. M.; Raja, R. *Stud. Surf. Sci. Catal.* **2004**, *148*, 163−211.
(8) Itoh, T.; Yano, K.; Inada, Y.; Fukushima, Y. *J. Am. Chem. Soc.* **2002**, *124*, 13437−13441.
(9) Mal, N. K.; Fujikawa, M.; Tanaka, Y. *Nature* **2003**, *421*, 350−353.
(10) Schüth, F.; Schmidt, W. *Adv. Mater.* **2002**, *14*, 629−638.
(11) Yamamoto, T.; Tanaka, T.; Funabiki, T.; Yoshida, S. *J. Phys. Chem. B* **1998**, *102*, 5830−5939.
(12) Inaki, Y.; Yoshida, H.; Kimura, K.; Inagaki, S.; Fukushima, Y.; Hattori, T. *Phys. Chem. Chem. Phys.* **2000**, *2*, 5293−5297.
(13) Iwamoto, M.; Tanaka, Y.; Sawamura, N.; Namba, S. *J. Am. Chem. Soc.* **2003**, *125*, 13032−13033.
(14) Junges, U.; Jacobs, W.; Voigt-Martin, I.; Krutzsch, B.; Schüth, F. *J. Chem. Soc., Chem. Commun.* **1995**, 2283−2284.
(15) Fukuoka, A.; Higashimoto, N.; Sakamoto, Y.; Inagaki, S.; Fukushima, Y.; Ichikawa, M. *Microporous Mesoporous Mater.* **2001**, *48*, 171−179.
(16) Fukuoka, A.; Sakamoto, Y.; Guan, S.; Inagaki, S.; Sugimoto, N.; Fukushima, Y.; Hirahara, K.; Iijima, S.; Ichikawa, M. *J. Am. Chem. Soc.* **2001**, *123*, 3373−3374.
(17) Sakamoto, Y.; Fukuoka, A.; Higuchi, T.; Shimomura, N.; Inagaki, S.; Ichikawa, M. *J. Phys. Chem. B* **2004**, *108*, 853−858.
(18) Fukuoka, A.; Higuchi, T.; Ohtake, T.; Oshio, T.; Kimura, J.; Sakamoto, Y.; Shimomura, N.; Inagaki, S.; Ichikawa, M. *Chem. Mater.* **2006**, *18*, 337−343.
(19) Rosso, I.; Galleitti, C.; Saracco, G.; Garrone, E.; Specchia, V. *Appl. Catal., B* **2004**, *48*, 195−203.
(20) Oh, S. H.; Sinkevitch, R. M. *J. Catal.* **1993**, *142*, 254−262.
(21) Kahlich, M. J.; Gasterger, H. A.; Behm, R. J. *J. Catal.* **1997**, *171*, 93−105.
(22) Minemura, Y.; Ito, S.; Miyao, T.; Naito, S.; Tomishige, K.; Kunimori, K. *Chem. Commun.* **2005**, 1429−1431.
(23) Pedrero, C.; Waku, T.; Iglesia, E. *J. Catal.* **2005**, *233*, 242−255.
(24) Pozdnyakova, O.; Teschner, D.; Wootsch, A.; Kröhnert, J.; Steinhauer, B.; Sauer, H.; Toth, L.; Jentoft, F. C.; Knop-Gericke, A.; Paál, Z.; Schlögl, R. *J. Catal.* **2006**, *237*, 1−16.
(25) Echigo, M.; Tabata, T. *Appl. Catal., A* **2003**, *251*, 157−166.
(26) Chilukuri, S.; Joseph, T.; Malwadkar, S.; Damle, C.; Halligudi, S. B.; Rao, B. S.; Sastry, M.; Ratnasamy, P. *Stud. Surf. Sci. Catal.* **2003**, *146*, 573−576.
(27) Landon, P.; Ferguson, J.; Solsona, B. E.; Garcia, T.; Carley, A. F.; Herzing, A. A.; Kiely, C. J.; Golunski, S. E.; Hutchings, G. J. *Chem. Commun.* **2005**, 3385−3387.
(28) Watanabe, M.; Uchida, H.; Ohkubo, K.; Igarashi, H. *Appl. Catal., B* **2003**, *46*, 595−600.

10.1021/ja0703123 CCC: $37.00

PROX catalysts, but their catalytic activity, selectivity, and durability need further improvement.

We explored the catalysis of Pt nanoparticles and nanowires synthesized in FSM-16 in the PROX reaction. Mesoporous silicas FSM-16 and MCM-41 are synthesized from different precursors, but they have the same structure (two-dimensional hexagonal structure (*p*6*mm* symmetry) of one-dimensional channels).[2,3] We also used mesoporous organosilica HMM-1 with bridging $-CH_2CH_2-$ groups[5] and conventional silica to know the effect of the organic group and the mesoporous structure on the catalytic performances. The Pt particles in FSM-16 exhibit catalytic behavior markedly different from that of Pt/SiO_2. Extremely high CO conversion and selectivity are obtained over Pt/FSM-16 at low temperature. The promotional effect of the mesoporous silica was further studied by infrared (IR) spectroscopy using isotopes of CO, O_2, and H_2, and we propose a reaction mechanism with the involvement of support-oxygen in the CO oxidation reaction.

2. Experimental Section

Preparation of Supported Pt Catalysts. FSM-16[2] and HMM-1[5] were synthesized according to the literature. SiO_2 (Fuji Silysia, Cariact Q-10) and γ-Al_2O_3 (Nishio, A-11) were used as received. Supported Pt catalysts were prepared as follows. Typically, FSM-16 (200 mg in 30 mL of water) was impregnated with $H_2PtCl_6{\cdot}6H_2O$ (Wako, 28 mg in 30 mL of water). The mixture was stirred for 24 h, evaporated to dryness, and dried under vacuum for 24 h. The resulting H_2PtCl_6/FSM-16 was calcined in O_2 flow at 473 K for 2 h, then reduced in H_2 flow at 473 K for 2 h to give Pt nanoparticles in FSM-16 (abbreviated Pt(p)/FSM-16). UV-irradiation (250−600 nm) to H_2PtCl_6/FSM-16 with water and methanol vapors for 48 h yielded Pt nanowires in FSM-16 (Pt(w)/FSM-16).[15] Pt particles and/or wires were also prepared in HMM-1. Pt/SiO_2 and Pt/Al_2O_3 were prepared by the similar impregnation and hydrogen-reduction. The Pt loading was 5 wt % for all of the catalysts.

Pt nanowires were extracted from FSM-16 with HF and again deposited on the external surface of FSM-16.[17,18] This material was also used as a catalyst: Pt(w,ex)/FSM-16.

Characterization. N_2 adsorption was carried out with a Quantachrome Autosorb-6, and uptakes of CO (323 K) and H_2 (298 K) were measured with a Quantachrome Chembet-3000. Powder X-ray diffraction (XRD) patterns were recorded on a Rigaku Miniflex using Cu Kα radiation ($\lambda = 0.15418$ nm) at 30 kV and 15 mV. Transmission electron microscopy (TEM) was performed with a Hitachi H-800 and a JEOL JEM-2000ES, and field-emission scanning electron microscopy (FE-SEM) with a Hitachi S-5500. X-ray photoelectron spectroscopy (XPS) was measured with a JEOL JPS-9010MC. Temperature-programmed desorption (TPR) of CO was analyzed using a Bell Japan TPD-1-AT.

IR spectra were measured at 293 K with a JASCO FTIR-420 spectrometer (resolution 2−4 cm^{-1}, integration 100 times). A self-supported wafer was prepared from catalyst powder (50 mg). The wafer sample was charged in an IR cell with CaF_2 windows, and dried under vacuum at 473 K for 30 min. Next, H_2 (100 Torr) was added to the cell, and the sample was reduced at 473 K for 1 h. After evacuation at 473 K for 30 min, the sample was cooled to 293 K, and IR spectra were acquired after exposure of the sample to CO or ^{13}CO for 10 min. Next, other gases (H_2, D_2, O_2, or $^{18}O_2$) were added to the cell, and IR spectra were similarly measured after 10 min. For each treatment, the IR spectrum was obtained by subtracting the spectrum of gaseous CO charged in the IR cell.

(29) Tanaka, K.; Moro-oka, Y.; Ishigure, K.; Yajima, T.; Okabe, Y.; Kato, Y.; Hamano, H.; Sekiya, S.; Tanaka, H.; Matsumoto, Y.; Koinuma, H.; He, H.; Zhang, C.; Feng, Q. *Catal. Lett.* **2004**, *92*, 115−121.

Table 1. Structural Parameters of Supports and Catalysts

materials	surface area (BET, $m^2\ g^{-1}$)[a]	pore diameter (BJH, nm)[b]	pore volume ($mL\ g^{-1}$)	CO/Pt	H/Pt
FSM-16	1018	2.7	0.84		
HMM-1	689	3.0	0.57		
SiO_2	287		1.33		
Al_2O_3	82		0.13		
Pt(p)/FSM-16	944	2.7	0.77	0.24	0.27
Pt(w)/FSM-16	878	2.7	0.68	0.09	0.08
Pt(w,ex)/FSM-16	979	2.7	0.78		
Pt(p)/HMM-1	661	3.0	0.58	0.31	
Pt(w)/HMM-1	648	3.0	0.57	0.15	0.15
Pt/SiO_2				0.13	0.11
Pt/Al_2O_3				0.17	

[a] Brunauer−Emmet−Teller surface area. [b] Barrett−Joyner−Halenda method.

PROX Reaction. Catalytic PROX reactions were conducted in a plug flow reactor (inner diameter 8 mm) made of Pyrex (Figure S1). Mass flows of CO (99.9%), H_2 (99.999%), O_2 (99.999%), N_2 (99.999%, internal standard), and CO_2 (99.95%) were controlled by mass flow controllers (STEC). Typically, Pt(p)/FSM-16 (0.1 g, Pt 5 wt %) was diluted with glass beads (diameter 1 mm, 1.5 g) and charged in the reactor. The catalyst was reduced in H_2 flow at 473 K for 1 h, treated in N_2 flow at 473 K for 30 min, and cooled to room temperature. Next, a gas mixture (CO 1%, O_2 0.5−1%, N_2 5%, H_2 balance, flow rate 20 mL min^{-1}, space velocity (SV) 12 000 mL $g^{-1}\ h^{-1}$, 0.1 MPa) was fed to the reactor. Reactions with CO_2 (20%) and water vapor (2%) were also performed by adjusting the flow rate of H_2, but SV was always kept constant under various conditions. After reaching to the steady state in ca. 1 h, the outlet gas was analyzed by on-line gas chromatography (Shimadzu GC 8A, thermal conductivity detector, a molecular sieve 13X column (4 m) for separation of H_2, O_2, N_2, and CO and an active carbon column (2 m) for CO_2, temperature 323−453 K (16 K min^{-1})). The CO conversion (X_{CO}) and the CO selectivity (S_{CO}) are defined as follows: $X_{CO} = (N_{CO,in} - N_{CO,out})/N_{CO,in} \times 100$ (%), $S_{CO} = (1/2)(N_{CO,in} - N_{CO,out})/(N_{O_2,in} - N_{O_2,out}) \times 100$ (%), where N is mol of CO or O_2.

3. Results and Discussion

3.1. Synthesis and Characterization of Pt Particles and Wires in Mesoporous Silica. Pt nanoparticles and nanowires were selectively synthesized by the typical impregnation and subsequent hydrogen- or photoreduction method.[15−18] Nitrogen adsorption isotherms for FSM-16 and Pt(p)/FSM-16 are shown in Figure S2, and structural parameters of the supports and catalysts are summarized in Table 1. TEM, SEM, and STEM data for the catalysts are shown in Figures 1 and S3. From these results, the formation of mesopores is clearly observed for FSM-16 and HMM-1, and similar pore diameters are obtained from the TEM and SEM images and the pore size distribution in the nitrogen adsorption.

For Pt(p)/FSM-16, the formation of 2.5 nm Pt particles is clearly observed in the TEM and STEM images (Figure 1a,d), and the SEM image (Figure 1c) shows no formation of big Pt particles on the external surface of FSM-16. These results indicate that the Pt particles are located in the internal mesopores. On the other hand, Pt wires (2.5 nm × 100−200 nm) were formed in FSM-16 by the photoreduction method (Figure 1b). We also synthesized Pt particles or wires in HMM-1 by the similar hydrogen- or photoreduction, and Pt particles on SiO_2 and Al_2O_3 by the hydrogen-reduction (TEM, Figure S3). In contrast to the mesoporous silica supports, a broad distribution of the particle size was observed for Pt/SiO_2 (3−7 nm) and Pt/Al_2O_3 (3−10 nm) in the TEM images.

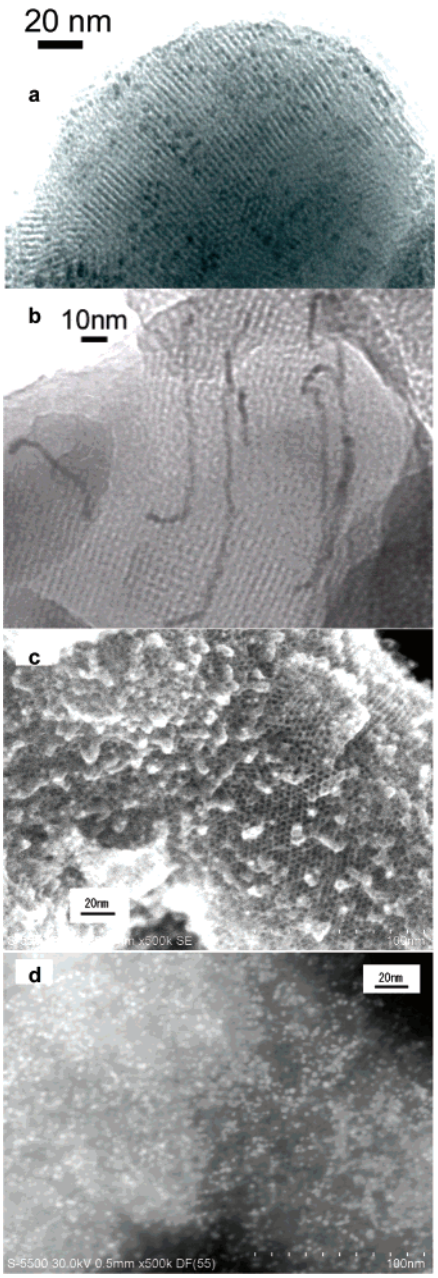

Figure 1. TEM images of (a) Pt(p)/FSM-16 and (b) Pt(w)/FSM-16. (c) High-resolution SEM image of Pt(p)/FSM-16 and (d) HAADF (high angle annular dark field) STEM image for (c).

As shown in Table 1, the dispersion of Pt is 24−27% for Pt(p)/FSM-16 and 8−9% for Pt(w)/FSM-16 by the uptake of CO and H_2. The TEM images in Figure 1 and the XRD data in Figure 2 (vide infra) indicate that the 2.5 nm fcc Pt particles are located in the mesopores of FSM-16. The ratio of surface to bulk is 45% for the 2.5 nm Pt particle with fcc lattice structure (truncated-cuboctahedron model).[30] By comparing this value (45%) and the dispersion data (24−27%), it is suggested that 50−60% of the Pt surface is exposed to the gas phase for Pt(p)/FSM-16. Similarly, ca. 25% of the Pt surface is exposed to the gas phase even for Pt(w)/FSM-16. If the Pt particle or wire plugged the mesopores, the dispersion would be markedly smaller than the experimental results. Therefore, our results suggest that the mesopores are not completely plugged by the Pt particles. It is thus reasonable to assume that the Pt particles and wires at the internal mesopores work as catalysts in the gas-phase reactions containing CO and H_2.

(30) Bergeret, G.; Gallezot, P. In *Handbook of Heterogeneous Catalysis*; Ertl, G., Knözinger, H., Weitkamp, J., Eds.; VCH: Weinheim, 1997; Vol. 1, p 439.

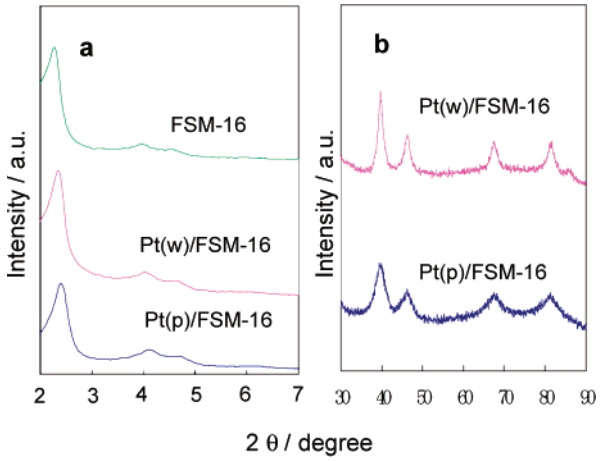

Figure 2. XRD patterns of FSM-16, Pt(p)/FSM-16, and Pt(w)/FSM-16 at high and low 2θ angles.

In the XRD patterns for Pt/FSM-16, no significant change was observed at a low 2θ angle (Figure 2a), indicating that the ordered mesoporous structure remains unchanged before and after the incorporation of Pt particles and wires. Peaks at a high 2θ angle in Figure 2b were assigned to typical fcc Pt by comparing with the JCPDS card (No. 04-0802). The XRD patterns for other catalysts are summarized in Figure S4.

3.2. Catalytic Performances of the Supported Pt Catalysts in the PROX Reactions. First, PROX reactions were carried out under the conditions of twice excess O_2 ($O_2/CO = 1$) over the stoichiometry ($CO + {}^1/_2O_2 \rightarrow CO_2$) according to the conditions of precedent papers.[19−27] Figure 3 shows the CO conversion over the supported Pt catalysts as a function of reaction temperature. Pt(p)/FSM-16 and Pt(w)/FSM-16 provided high CO conversions, while SiO_2-, Al_2O_3-, and HMM-1-supported catalysts needed 423 K for removal of a majority of CO. In particular, Pt(p)/FSM-16 gave ca. 100% conversion of CO even at 313 K, thus showing that this is one of the most active catalysts for PROX. No decrease in the CO conversion was observed over Pt(p)/FSM-16 under the practical condition containing CO_2 (20%) and water vapor (2%) at 333 K (▼ in Figure 3a).

It is a task for the PROX catalysts to work only for CO oxidation in the presence of excess H_2, because the H_2 oxidation ($H_2 + {}^1/_2O_2 \rightarrow H_2O$) is a competitive reaction. The stoichiometric condition ($O_2/CO = {}^1/_2$) is enough for the CO oxidation alone, but excess O_2 is needed for high conversion of CO due to the consumption of O_2 in the H_2 oxidation. Hence, the selectivity for CO oxidation (CO selectivity) is an important factor to evaluate the performances of PROX catalysts, where the CO selectivity is defined as the ratio of the consumed CO to the consumed O_2 (see Experimental Section). In our reactions flowing the stoichiometric O_2/CO ($^1/_2$) gas mixture, Pt(p)/FSM-16 showed CO conversions over 95% at 298−423 K, while Pt/SiO_2 gave low conversions (Figure 3b). This indicates that the CO selectivity is over 95% for Pt(p)/FSM-16. The CO selectivity was also studied under excess O_2 ($O_2/CO = 1$) by keeping the O_2 conversion at 20−40% at various temperature.

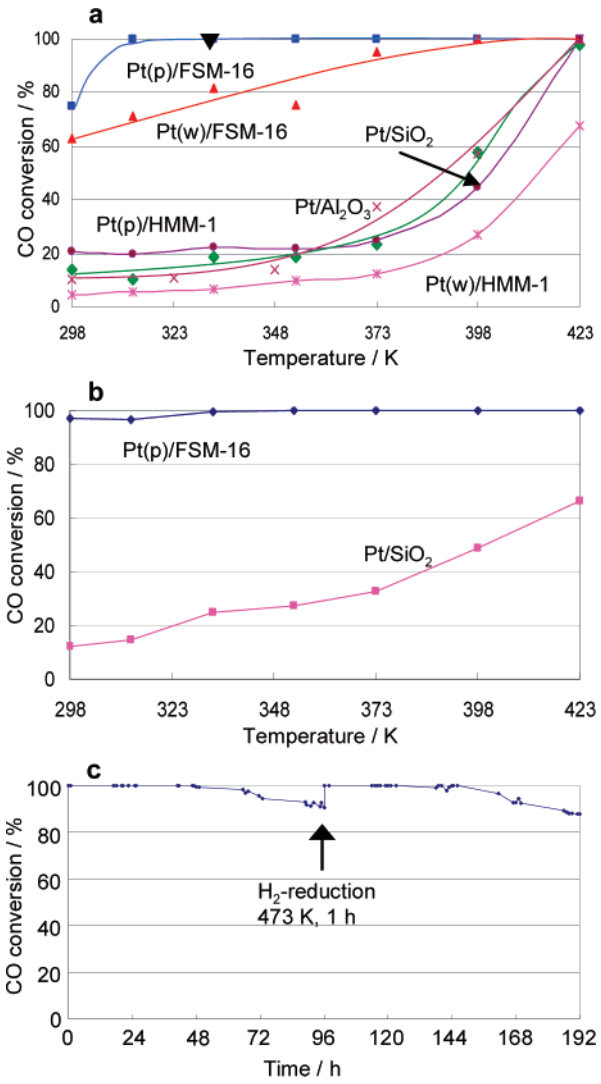

Figure 3. PROX reactions over supported Pt catalysts. (a) Under $O_2/CO = 1$. (b) Under stoichiometric $O_2/CO = {}^1/_2$. (c) Durability test of Pt(p)/FSM-16 at 353 K under $O_2/CO = 1$. Conditions: CO 1%, O_2 0.5−1%, N_2 5%, H_2 balance, SV 12 000 mL g^{-1} h^{-1}, 0.1 MPa.

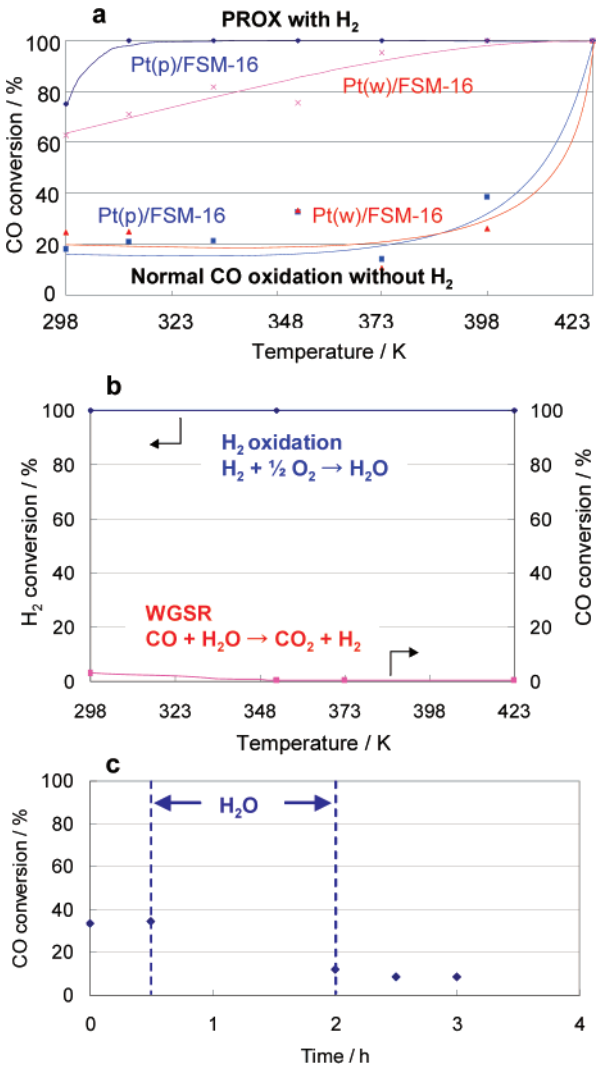

Figure 4. (a) PROX and normal CO oxidation over Pt(p)/FSM-16. Conditions of PROX: CO 1%, O_2 1%, N_2 5%, H_2 (PROX) or He (normal CO oxidation) balance, SV 12 000 mL g^{-1} h^{-1}, 0.1 MPa. (b) H_2 oxidation and water-gas shift reaction over Pt(p)/FSM-16. Conditions of H_2 oxidation: O_2 1%, N_2 5%, H_2 balance, SV 12 000 mL g^{-1} h^{-1}, 0.1 MPa. Conditions of WGSR: CO 1%, H_2O 2%, N_2 5%, He balance, SV 12 000 mL g^{-1} h^{-1}, 0.1 MPa. (c) Addition of water to normal CO oxidation over Pt(p)/FSM-16 at the reaction time of 0.5−2.0 h. Conditions: CO 1%, O_2 1%, H_2O 2%, N_2 5%, He balance, SV 12 000 mL g^{-1} h^{-1}, 0.1 MPa, 333 K.

As depicted in Figure S5, high selectivity was obtained over the Pt catalysts on FSM-16 and HMM-1, but Pt/SiO_2 or Al_2O_3 showed 50−60% selectivity.

In the durability test of Pt(p)/FSM-16 at 353 K (Figure 3c), the CO conversion decreased slightly from 100% to 90% in 96 h, but the catalyst was regenerated by the hydrogen-reduction at 473 K for 1 h. No sintering of Pt particles or wires was observed in the recovered catalysts (Figure S6). Because of the high activity, selectivity, and durability of Pt(p)/FSM-16, we can operate the PROX reaction at 313−353 K, which would be beneficial to the production of hydrogen for fuel cells by reducing the number of cooling processes.[19] The catalytic performances of Pt(p)/MCM-41 were the same as those of Pt(p)/FSM-16, thus making no difference between FSM-16 and MCM-41 as a support. It is reported that Pt−Fe/mordenite showed high conversion and selectivity below 353 K,[28] but this catalyst was not durable as described in ref 27, giving lower conversion and selectivity than Pt(p)/FSM-16 in our test reactions.

To elucidate the effect of the internal and external surfaces of FSM-16, Pt wires were extracted from Pt(w)/FSM-16 by dissolving silica with HF and the wires were again deposited on FSM-16.[17,18] However, the resulting Pt(w,ex)/FSM-16 gave lower activity and selectivity than Pt(w)/FSM-16 (Figure S7), which indicates that the occlusion of Pt in the internal pores is important for high performances.

Under the normal CO oxidation conditions using He flow instead of H_2, the CO conversion declined to 20% over Pt/FSM-16 catalysts (Figure 4a), showing that H_2 has a promotional effect on the CO oxidation. One explanation for the H_2 effect is the involvement of the water-gas shift reaction (WGSR: $CO + H_2O \rightarrow CO_2 + H_2$). However, Pt(p)/FSM-16 was active for the H_2 oxidation but inactive for WGSR (Figure 4b). Furthermore, the addition of H_2O to the normal CO oxidation over Pt(p)/FSM-16 had no positive effect on the CO conversion (Figure 4c). These results indicate that H_2O is not involved in the PROX mechanism by Pt(p)/FSM-16.

3.3. Mechanistic Study of the PROX Reaction by IR. We have studied the PROX mechanism by IR spectroscopy. Figure

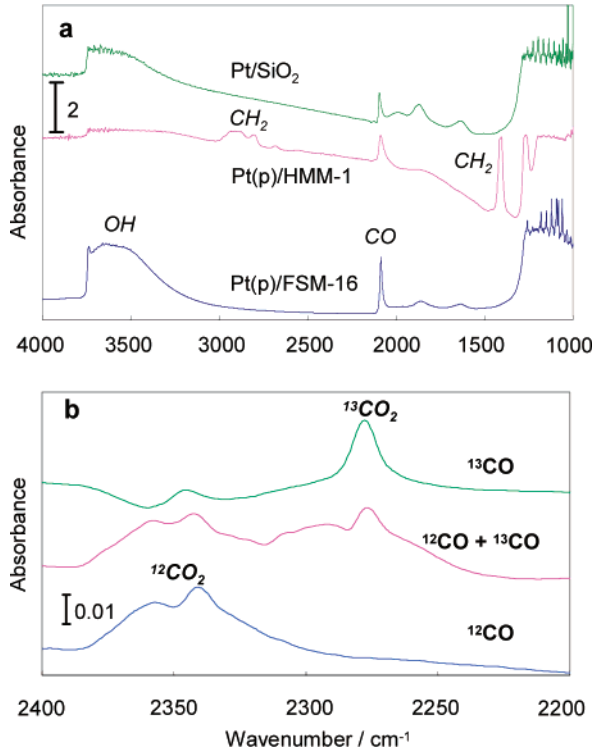

Figure 5. IR spectra of CO adsorption on supported Pt catalysts. (a) CO (30 Torr) at 293 K. (b) Gaseous $^{12}CO_2$ or $^{13}CO_2$ formed in the adsorption of ^{12}CO (30 Torr) and/or ^{13}CO (30 Torr) on Pt(p)/FSM-16.

5a shows the IR spectra of the supported Pt catalysts after addition of CO (30 Torr, 1 Torr = 133 Pa) at 293 K. All three samples, active Pt(p)/FSM-16 and inactive Pt(p)/HMM-1 and Pt/SiO_2, showed a linear CO frequency on Pt at 2088 cm^{-1}, indicating no difference in the electronic states at the Pt surfaces. The XPS results (Figure S8) and the TPD of CO (Figure S9) also indicate the similar electronic states of the three catalysts. In the enlarged IR spectrum for Pt/(p)/FSM-16 at 2400−2200 cm^{-1} (Figure 5b), small gaseous CO_2 peaks were observed at ca. 2350 cm^{-1}. In the adsorption of ^{13}CO or a mixture of ^{12}CO and ^{13}CO, gaseous $^{13}CO_2$ peak was seen at 2280 cm^{-1}. It should be noted that no oxygen source was present except for the support FSM-16 in the adsorption of ^{12}CO or ^{13}CO. One possible explanation is that the oxygen of silica in FSM-16 is incorporated into CO_2 in the CO adsorption. In contrast to the active Pt(p)/FSM-16, no CO_2 peaks were observed in the CO adsorption over the inactive Pt(p)/HMM-1 or Pt/SiO_2 catalyst.

To confirm the incorporation of the oxygen of FSM-16 into CO_2, we carried out sequential addition of CO, $^{18}O_2$, and D_2 on Pt(p)/FSM-16. After admission of CO (10 Torr) to the IR cell at 293 K, gaseous $C^{16}O_2$ was formed as shown in Figure 6a. By further addition of $^{18}O_2$ (10 Torr) to the cell, the peak intensity of $C^{16}O_2$ slightly increased, but no peak of $C^{16}O^{18}O$ was detected at 2330 cm^{-1} as an ^{18}O-labeled CO_2. After introduction of D_2 (60 Torr) to make the PROX conditions (CO + $^{18}O_2$ + D_2), the $C^{16}O_2$ peak again increased but the peaks of ^{18}O-labeled CO_2 were not observed. If labeled water ($D_2{}^{18}O$) generated from D_2 and $^{18}O_2$ attacked CO, $C^{16}O^{18}O$ would be a main product of WGSR. Therefore, neither gas-phase oxygen ($^{18}O_2$) nor water ($D_2{}^{18}O$) reacts with $C^{16}O$ over Pt(p)/FSM-16, and the surface silanol groups are the source of oxygen in the CO oxidation.

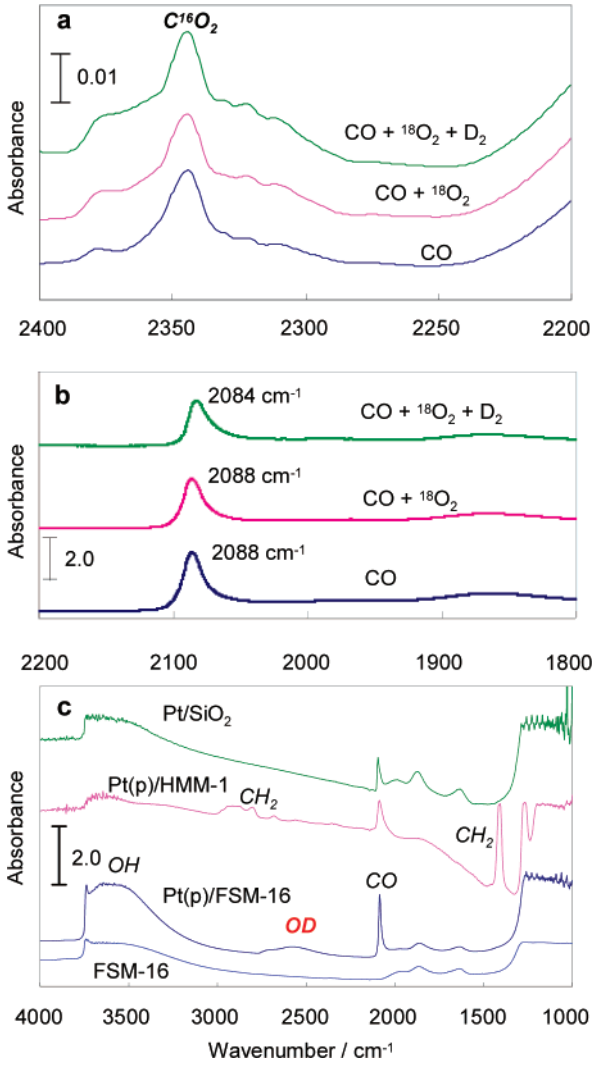

Figure 6. IR spectra of gaseous CO_2 (a) and Pt−CO (b) in sequential adsorption of CO (10 Torr), $^{18}O_2$ (10 Torr), and D_2 (60 Torr) on Pt(p)/FSM-16 at 293 K. (c) IR spectra in sequential adsorption of CO (10 Torr) and D_2 (10 Torr) on various supported Pt catalysts at 293 K.

Figure 6b shows the change of Pt−CO peak in the sequential adsorption of CO, $^{18}O_2$, and D_2 on Pt(p)/FSM-16. The Pt−D peak was not directly observed due to the overlap with strong Pt−CO peak. Even in the adsorption of H_2 or D_2 alone, the Pt−H or Pt−D peaks were not observed in IR. However, we have observed the shift of Pt−CO peak that suggests the site-selective adsorption of H_2 on Pt and O_2 on FSM-16. After admission of CO to Pt(p)/FSM-16, the Pt−CO peak appeared at 2088 cm^{-1} and the peak was not shifted by the addition of $^{18}O_2$ to the gas phase (Figure 6b). In contrast, by further addition of D_2 to the gas phase, the Pt−CO peak was shifted to 2084 cm^{-1}. This low-frequency shift is attributable to the enhanced back-donation from Pt to CO by forming a Pt−D bond in the dissociative adsorption of D_2 to Pt. If $^{18}O_2$ were adsorbed on Pt under the same conditions, the Pt−CO peak would be shifted to higher frequency by the decreased back-donation from Pt to CO. Accordingly, we conclude that oxygen is not adsorbed on Pt but on the support FSM-16.

We also tested the possibility of fast $^{16}O-{}^{18}O$ exchange between gaseous $C^{18}O_2$ and siliceous FSM-16 ($Si^{16}O_2$), but no exchange was observed in the admission of $C^{18}O_2$ to Pt(p)/FSM-

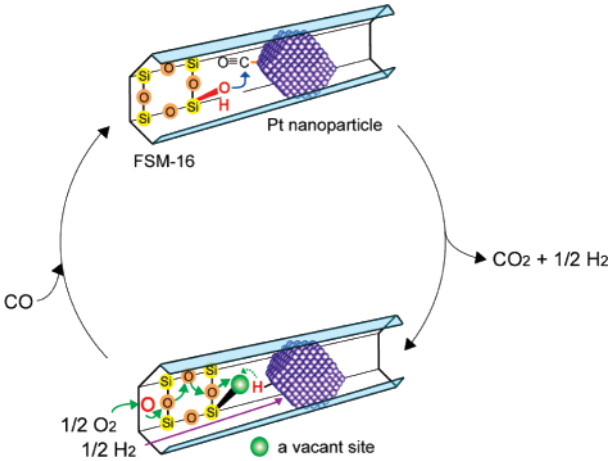

Figure 7. Proposed mechanism for PROX over Pt(p)/FSM-16.

16 (Figure S10). It is thus reasonable to conclude that the oxygen of FSM-16 is incorporated into CO_2 even at 293 K.

As shown in Figure 5a, Pt(p)/FSM-16 gave more OH groups at 3800−3200 cm^{-1} than did Pt/SiO_2 and Pt(p)/HMM-1. When D_2 was admitted to the IR cell after CO adsorption at 293 K, a broad band of OD was detected over Pt(p)/FSM-16 at ca. 2600 cm^{-1} (Figure 6c), while the OD band was not seen over Pt/SiO_2, Pt(p)/HMM-1, or FSM-16 itself. Presumably D_2 is dissociatively adsorbed on the Pt surface even in the presence of adsorbed CO, and the resulting D species spills over onto the FSM-16 surface to be exchanged with the surface OH. We found that Pt(p)/FSM-16 are active for both the H−D exchange and the PROX reaction.

By considering the catalytic performances and the IR results, we propose that the surface OH on FSM-16 is highly reactive toward CO adsorbed on Pt nanoparticles at the interface of Pt and FSM-16. As depicted in Figure 7, the OH groups attack CO on Pt to form CO_2 and H_2, and a vacant site is formed on FSM-16. O_2 is adsorbed on FSM-16 as shown in Figure 6, and it is suggested that the oxygen species migrates in FSM-16 to form the OH groups with spill-over hydrogen from Pt. In this mechanism, CO reacts with surface OH instead of H_2O. Basset et al. also reported that silanol groups (Si−^{18}OH) of conventional silica react with bis(allyl)Rh complex immobilized on the silica to form Rh(C^{18}O) complex.[31] This also indicates the attack of silanol groups on the surface species on metal at the interface of metal and support. In our experiments, the mesoporous silica has a greater effect on the PROX reaction than the conventional silica (Figure 3a), thus showing that the OH groups at the internal surface of mesoporous silica are more active than those of the conventional silica.

If O_2, H_2, and CO were competitively adsorbed on Pt, the formation of H_2O would not be avoided to reduce the CO selectivity. Hence, the key to the high CO selectivity over Pt(p)/FSM-16 is the site-selective adsorption of H_2 on Pt and O_2 on FSM-16 without the formation of H_2O. Tanaka et al. reported that a small amount of H_2O works as a cocatalyst for PROX over $FeO_x/Pt/TiO_2$ catalyst.[32] In contrast to this catalyst, the addition of H_2O showed no improvement of CO oxidation over Pt(p)/FSM-16 (Figure 4c). If H_2O were formed, the CO selectivity would be lower in the catalytic reactions, and C^{16}O^{18}O would be formed from C^{16}O and $D_2{}^{18}$O in the sequential adsorption of CO, $^{18}O_2$, and D_2. Therefore, it seems unlikely that water is involved in our PROX mechanism.

4. Conclusion

We have shown that mesoporous silica-supported Pt nanoparticles are highly active and selective catalysts in the PROX of CO. The catalytic performances of supported Pt catalysts are promising with an impact at the commercial level. We have also demonstrated the incorporation of support-oxygen into the product CO_2 by the IR experiments using the isotopic tracer technique. From the experimental results, we conclude that the PROX is promoted by the attack of OH groups at the internal surface of mesoporous silica toward CO on Pt. The high activity of the surface OH groups would be applicable to other oxidation reactions. Work along this line is now in progress.

Acknowledgment. We thank Mr. Y. Nodasaka for TEM, Hitachi High-Technologies for FE-SEM, Dr. N. Iwasa for TPD, and Dr. S. Inagaki, Prof. K. Tanaka, Dr. K. Yamakata, and Dr. P. L. Dhepe for discussions on the reaction mechanism. This work was supported by a Grant-in-Aid for Scientific Research from the Ministry of Education, Culture, Sports, Science and Technology, Japan (18560737, 18065001), and NOASTEC.

Supporting Information Available: Schematic representation of the plug flow reactor (Figure S1); nitrogen adsorption isotherms for FSM-16 and Pt(p)/FSM-16 (Figure S2); TEM (Figure S3) and XRD (Figure S4) of Pt/HMM-1, Pt/Al_2O_3, and Pt/SiO_2; CO selectivity at 20−40% O_2 conversion over the supported Pt catalysts (Figure S5); TEM of the recovered Pt(p) or Pt(w)/FSM-16 after PROX (Figure S6); PROX by Pt(w,ex)/FSM-1 (Figure S7); XPS of Pt(p)/FSM-16 (Figure S8); TPD of CO for the supported Pt catalysts (Figure S9); and IR of C$^{18}O_2$ adsorption on Pt(p)/FSM-16 (Figure S10). This material is available free of charge via the Internet at http://pubs.acs.org.

JA0703123

(31) Santini, C. C.; Scott, S. L.; Basset, J.-M. *J. Mol. Catal. A* **1996**, *107*, 263−271.

(32) Tanaka, K.; Shou, M.; He, H.; Shi, X. *Catal. Lett.* **2006**, *110*, 185−190.